ORIGINAL ARTICLE

Synthesis, characterization, density functional study and antimicrobial evaluation of a series of bischelated complexes with a dithiocarbazate Schiff base ligand

CrossMark

E. Zangrando [a], M.S. Begum [b],*, M.C. Sheikh [c], R. Miyatake [d], M.M. Hossain [e], M.M. Alam [b], M.A. Hasnat [b], M.A. Halim [f,g], S. Ahmed [h], M.N. Rahman [h], A. Ghosh [h]

[a] *Department of Chemical and Pharmaceutical Sciences, Via L. Giorgieri 1, 34127 Trieste, Italy*
[b] *Department of Chemistry, Shahjalal University of Science and Technology, Sylhet 3114, Bangladesh*
[c] *Department of Applied Chemistry, Faculty of Engineering, University of Toyama, 3190 Gofuku, Toyama 930-8555, Japan*
[d] *Center for Environmental Conservation and Research Safety, University of Toyama, 3190 Gofuku, Toyama 930-8555, Japan*
[e] *Department of Chemistry, Rajshahi University, Rajshahi 6205, Bangladesh.*
[f] *Bangladesh Institute of Computational Chemistry and Biochemistry, 38 Green Road West, Dhaka 1205, Bangladesh*
[g] *Institut Lumière Matière, Université Lyon 1 – CNRS, Université de Lyon, 69622 Villeurbanne Cedex, France*
[h] *Department of Biochemistry and Molecular Biology, Shahjalal University of Science and Technology, Sylhet 3114, Bangladesh*

Abstract A nitrogen-sulfur Schiff base HL (**1**) derived from S-hexyldithiocarbazate and 4-methylbenzaldehyde has been reacted with different divalent metal ions in 2:1 molar ratio, producing neutral complexes (**2–7**) of general formula $M^{II}L_2$ (where M = Ni, Cu, Zn, Cd, Pd and Pb). All compounds were characterized using established physico-chemical and spectroscopic methods. The single crystal structures of Cu^{II} and Zn^{II} complexes are compared and discussed with those of Ni^{II} and Pd^{II} already reported by us, underlining the geometrical variations occurring in the HL ligand upon coordination. The metal complexes, as revealed by the X-ray diffraction analyses, show a square planar or tetrahedral coordination geometry, and in the former case either a *cisoid* or *transoid* configuration of chelating ligands. Density functional theory (DFT) and time-dependent density functional theory (TD-DFT) calculations have been performed on the isolated *cis/trans*

---

* Corresponding author. Fax: +880 821 715257.
  E-mail address: sabina_sust@yahoo.com (M.S. Begum).
Peer review under responsibility of King Saud University.

ELSEVIER | **Production and hosting by Elsevier**

complexes of Ni and Pd complexes in order to evaluate the stability of the isomer isolated in solid state. The thermodynamic parameters for *trans* to *cis* isomerization of NiL_2 complex [$\Delta H = -29.12$ kJ/mol and $\Delta G = -43.97$ kJ/mol] indicated that the *trans* isomer (observed in solid state) is more stable than the *cis* one. On the other hand, relative enthalpy [$\Delta H = -4.37$ kJ/mol] and Gibbs free energy [$\Delta G = -5.50$ kJ/mol] of PdL_2 complex disclosed a small difference between the energies of the two isomers. Experimental UV–vis and TD-DFT calculation confirmed that these complexes have distinctive LMCT bands with a broad shoulder at 400–550 nm. With the purpose of providing insight into the properties and behavior of the complexes in solution, photoluminescence and electrochemical experiments have been also performed. Finally, the anti-bacterial activity of these compounds was evaluated against three pathogenic Gram-negative organisms such as *Escherichia coli*, *Salmonella typhi* and *Shigella flexneri*, but only the free ligand **1** showed anti-bacterial property against all three tested organisms.

1. Introduction

Transition metal complexes derived from Schiff bases have occupied a central role in the development of coordination chemistry. Thiosemicarbazones, semicarbazones, hydrazide/hydrazones and dithiocarbazates are compounds that have been widely studied since they exhibit significant biological and pharmacological properties (Pavan et al., 2010). In particular thiosemicarbazones have acquired considerable attention by medicinal chemists being excellent chelators of transition metals for their antitumor activity in vitro and in vivo (Yu et al., 2009; Richardson et al., 2006). The present work deals with hydrazine carbodithioate species that upon complexation typically act as bidentate ligands and coordinate through the β-nitrogen and the thiolate sulfur donors yielding air stable metal complexes. Schiff bases derived from hydrophobic *S*-alkyl/aryl groups and their complexes reveal promising potential applications (Beshir et al., 2008). In fact the reaction of dithiocarbazates with different aldehydes and ketones leads to ligands with modified donor properties, bringing about intriguing coordination geometries in metal complexes, a feature that affects also the bioactivity of these compounds such as antibacterial, antifungal, anticancer, antitumor, wound healing, cell motility as well as antioxidant activities (Beshir et al., 2008; Ali et al., 2002; Tampouris et al., 2007; da S. Maia et al., 2010; Singh et al., 2009). Surprisingly a bis-dithiocarbazate nickel complex has been recently tested also for the photocatalytic production of hydrogen (Wise et al., 2015).

A search in the Cambridge Structural Database (Groom et al., 2016) indicates that the majority of previous studies were based on Schiff bases derived from *S*-methyl, *S*-benzyl and *S*-acetyl dithiocarbazate and *N*-substituted derivatives of *S*-methyl dithiocarbazates, and only a few works reported on Schiff bases having long *S*-alkyl chain moiety. In addition Schiff bases derived from a large number of carbonyl compounds with dithiocarbazates have been synthesized, but the study of their optical properties, such as fluorescence, is more scarce (Singh et al., 2009). Therefore, considering the above facts and continuing our interest in this field, the present work reports a study on the synthesis, characterization and anti-bacterial properties of Ni, Cu, Zn, Cd, Pd and Pb complexes with the Schiff base derived from S-hexyldithiocarbazate and 4-methylbenzaldehyde (HL). Since the X-ray single crystal structure of square planar complexes (Ni, Cu and Pd) shows *cis* or *trans* configuration of the ligands, density functional theory (DFT) and time-dependent density functional theory (TD-DFT) calculations have been performed on the cis/trans isomers of Ni and Pd complexes with the purpose of elucidating the stability of the isomers isolated in solid state. The fluorescence properties of all the compounds and the electrochemical behavior of Ni^{II}, Cu^{II}, Pd^{II} and Pb^{II} complexes have also been studied.

2. Experimental and computational methods

2.1. Materials and physical measurements

4-Methylbenzaldehyde was purchased from British Drug House (BDH), England. Ethanol was distilled prior to use. IR spectra (4000–225 cm^{-1}) were obtained as KBr disk using a FT-IR 8400-Shimadzu spectrophotometer (Japan). ^{1}H NMR (500 MHz) and ^{13}C NMR (125 MHz) spectra were recorded on a JEOL JNM-A400 spectrometer in $CDCl_3$ with TMS as internal standard. Mass spectra were obtained on a JEOL-JMS-D300 mass spectrometer University of Toyama, Japan. Magnetic measurements were made on a magnetic susceptibility balance (Sherwood Scientific, UK) and molar conductance measurements with a heavy-duty conductivity meter (Extech Instruments, USA, model No. 407303). The UV–visible absorptions were scanned on a T60 UV–vis spectrophotometer (PG Instruments, UK) between 200 and 800 nm of 10^{-5} M solution in chloroform. Melting points were carried out on a melting point apparatus, Gallenkamp, England. Cyclic voltammogram was recorded on a CHI602 E electrochemical analyzer with three compartments. Fluorescence spectra were recorded on a Shimadzu RF-5301 PC spectrofluorophotometer.

2.2. Synthesis of the Schiff base ligand, 1

As previously reported (Howlader et al., 2015a), hydrazine hydrate (2.50 g, 0.05 mol, 99%) was added to an absolute ethanolic solution of KOH (2.81 g, 0.05 mol) and the mixture was stirred at 0 °C. To this solution carbon disulfide (3.81 g, 0.05 mol) was added dropwise with constant stirring for one hour. Then 1-bromohexane (8.25 g, 0.05 mol) was added dropwise at 0 °C with vigorous stirring for another hour. Finally, 4-methylbenzaldehyde (6.00 g, 0.05 mol) in ethanol (2.0 ml) was added and the mixture refluxed for 30 min. The hot mixture was filtered and then the filtrate cooled to 0 °C to give a precipitate of the Schiff base product, which was recrystallized from ethanol at room temperature and dried in a vacuum desiccator over anhydrous $CaCl_2$. The physical and spectroscopic data of the Schiff base ligand **1** are as follows:

Colorless, Yield: 75%; m.p. (83–85 °C). Selected IR data (KBr disk, cm^{-1}): ν(N—H) 3101 m, ν(C—H, alkyl) 2929 m, ν

(C=N) 1619 s, ν(C=S) 1101 s, ν(N−N) 1026 s, ν(CSS) 871 m. ^{1}H NMR (500 MHz, CDCl$_3$, ppm) δ: 11.01(s,1H, NH), 7.93(s, 1H, CH=N), 7.62(d, 2H, C-4,6), 7.21(d, 2H, C-3,7), 3.31(t, 2H, -SCH$_2$), 2.42(s, 3H, C-1), 1.76(p, 2H, C-11), 1.47(p, 2H, C-12), 1.34(m, 4H, C-13,14), 0.91(t, 3H, C-15). ^{13}C NMR (125 MHz, CDCl$_3$, ppm) δ: 199.33(C=S), 162.04(CH=N), 141.84(C-5), 129.66(C-4,6), 128.69(C-2), 127.99(C-3,7), 34.68 (C-1), 31.53(C-10), 28.85(C-11), 28.67(C-12), 22.66(C-13), 21.74(C-14), 14.17(C-15). UV–vis spectrum [CHCl$_3$, λ$_{max}$ nm (log ε, L mol^{-1} cm^{-1})]: 241(4.05), 262(4.0), 325(4.30), 338 (4.32). HRMS (FAB) Calc. for C$_{15}$H$_{23}$N$_2$S$_2$ (M + 1): 295.1224; Found (M + 1): 295.1302.

2.3. Synthesis of metal complexes, 2–7

Details of the synthesis of metal complexes **2** and **6** have been formerly reported (Howlader et al., 2015b; Begum et al., 2015). For complex **2** a solution of Ni(CH$_3$COO)$_2$·4H$_2$O (0.06 g, 0.25 mmol, 8 mL methanol) was added to a methanolic solution (10 mL) of the ligand (0.15 g, 0.5 mmol). The resulting mixture was stirred at room temperature for four hours. A dark reddish brown precipitate was formed, filtered off, washed with methanol and dried in vacuo over anhydrous CaCl$_2$ as complex **2**.

The corresponding Cu^{II}, Zn^{II}, Cd^{II}, Pd^{II} and Pb^{II} complexes (**3**–**7**) were prepared following the same procedure as described for **2** by using Cu(CH$_3$COO)$_2$·H$_2$O, Zn(CH$_3$COO)$_2$·2H$_2$O, Cd(CH$_3$COO)$_2$·3H$_2$O, PdCl$_2$ and Pb(CH$_3$COO)$_2$·3H$_2$O, respectively. The products were recrystallized from a mixture of chloroform and acetonitrile (5:1).

Dark reddish brown and orange red single crystals of Ni^{II} and Pd^{II} complexes, respectively, suitable for X-ray diffraction analysis, were obtained by slow evaporation from a mixture of chloroform and acetonitrile (1:1) after a week. Brown single crystals of CuL$_2$ and yellow ones of ZnL$_2$ were obtained at room temperature by slow evaporation from a mixture of chloroform/ acetonitrile (3:1) and of dichloromethane/acetonitrile (4:1), respectively. The physical and spectroscopic data of all compounds **2**–**7** are given below:

2.3.1. [NiL$_2$] (2)
Dark reddish brown, Yield: 65%; m.p. (100–102 °C). Selected IR data (KBr disk, cm^{-1}): ν(C−H, alkyl) 2914 m, ν(C=N) 1604 s, ν(N−N) 1030 s, ν(CSS) 803 m. ^{1}H NMR (500 MHz, CDCl$_3$, ppm) δ: 7.67 (s, 2H, CH=N), 7.88 (d, 4H, C-4,6), 7.19 (d, 4H, C-3,7), 3.12 (t, 4H, -SCH$_2$), 2.38 (s, 6H, C-1), 1.74 (p, 4H, C-11), 1.43 (p, 4H, C-12), 1.30 (m, 8H, C-13,14), 0.88 (t, 6H, C-15). UV–vis spectrum [CHCl$_3$, λ$_{max}$ nm (log ε, L mol^{-1} cm^{-1})]: 241(4.33), 291(4.47), 338(4.57), 382 (4.17), 443(3.91). HRMS (FAB) Calc. for C$_{30}$H$_{43}$N$_4$S$_4$Ni (M + 1): 645.1646; Found (M + 1): 645.1728. Molar conductivity (1.0 × 10^{-5} M; CHCl$_3$, Ω^{-1} cm^2 mol^{-1}): 0.00; μ$_{eff}$ = Diamagnetic.

2.3.2. [CuL$_2$] (3)
Reddish brown, Yield: 61%; m.p. (102–105 °C). Selected IR data (KBr disk, cm^{-1}): ν(C−H, alkyl) 2926 m, ν(C=N) 1583 s, ν(N−N) 1031 s, ν(CSS) 804 m. UV–vis spectrum [CHCl$_3$, λ$_{max}$ nm (log ε, L mol^{-1} cm^{-1})]: 244 (4.10), 271 (4.16), 324 (4.56), 376 (4.09), 443 (3.29). HRMS (FAB) Calc. for C$_{30}$H$_{43}$N$_4$S$_4$Cu (M + 1): 650.1588; Found (M + 1):

650.1664. Molar conductivity (1.0 × 10^{-5} M; CHCl$_3$, Ω^{-1} cm^2 mol^{-1}): 0.00; μ$_{eff}$ = 1.82 B.M.

2.3.3. [ZnL$_2$] (4)
Pale yellow, Yield: 55%; m.p. (125–127 °C). Selected IR data (KBr disk, cm^{-1}): ν(C−H, alkyl) 2924 m, ν(C=N) 1601 s, ν(N−N) 1041 s, ν(CSS) 811 m. ^{1}H NMR (500 MHz, CDCl$_3$, ppm) δ: 7.67 (s, 2H, CH=N), 8.12 (d, 4H, C-4,6), 7.27 (d, 4H, C-3,7), 3.24 (t, 4H, -SCH$_2$), 2.40(s, 6H, C-1), 1.80 (p, 4H, C-11), 1.47 (p, 4H, C-12), 1.33 (m, 8H, C-13,14), 0.88 (t, 6H, C-15). ^{13}C NMR (125 MHz, CDCl$_3$, ppm) δ: 184.77 (C=S), 163.06(CH=N), 143.43(C-5), 133.48(C-4,6), 129.40 (C-3,7), 128.61(C-2), 32.96(C-1), 31.56(C-10), 29.37(C-11), 28.77(C-12), 22.74(C-13), 21.94(C-14), 14.20(C-15). UV–vis spectrum [CHCl$_3$, λ$_{max}$ nm (log ε, L mol^{-1} cm^{-1})]: 238 (4.12), 267 (4.23), 322 (4.39), 355 (4.35), 435 (4.57). HRMS (FAB) Calc. for C$_{30}$H$_{43}$N$_4$S$_4$Zn (M + 1): 651.1584; Found (M + 1): 651.1659. Molar conductivity (1.0 × 10^{-5} M; CHCl$_3$, Ω^{-1} cm^2 mol^{-1}): 0.00; μ$_{eff}$ = Diamagnetic.

2.3.4. [CdL$_2$] (5)
Yellow, Yield: 48%; m.p. (136–138 °C). Selected IR data (KBr disk, cm^{-1}): ν(C−H, alkyl) 2918 m, ν (C=N) 1590 s, ν(N−N) 1034 s, ν(CSS) 810. ^{1}H NMR (500 MHz, CDCl$_3$, ppm) δ: 7.79 (s, 2H, CH=N), 7.95 (d, 4H, C-4,6), 7.20 (d, 4H, C-3,7), 3.01 (t, 4H, −SCH$_2$), 2.36 (s, 6H, C-1), 1.70 (p, 4H, C-11), 1.61 (p, 4H, C-12), 1.27 (m, 8H, C-13,14), 0.87 (t, 6H, C-15). ^{13}C NMR (125 MHz, CDCl$_3$, ppm) δ: 176.19(C=S), 162.26(CH=N), 142.51(C-5), 130.35(C-4,6), 128.29(C-3,7), 129.32(C-2), 35.64 (C-1), 32.54(C-10), 31.52(C-11), 29.65(C-12), 22.69(C-13), 21.74(C-14), 14.17(C-15). UV–vis spectrum [CHCl$_3$, λ$_{max}$ nm (log ε, L mol^{-1} cm^{-1})]: 244(4.15), 338(4.85). HRMS (FAB) Calc. for C$_{30}$H$_{43}$N$_4$S$_4$Cd (M + 1): 701.1326; Found (M + 1): 701.1411. Molar conductivity (1.0 × 10^{-5} M; CHCl$_3$, Ω^{-1} cm^2 mol^{-1}): 0.00; μ$_{eff}$ = Diamagnetic.

2.3.5. [PdL$_2$] (6)
Orange red, Yield: 64%; m.p. (159–161 °C). Selected IR data (KBr disk, cm^{-1}): ν(C−H, alkyl) 2926 m, ν(C=N) 1596 s, ν(N−N) 1031 s, ν(CSS) 813 m. ^{1}H NMR (500 MHz, CDCl$_3$, ppm) δ: 7.62 (s, 2H, CH=N), 7.53 (d, 4H, C-4,6), 7.14 (d, 4H, C-3,7), 3.06 (t, 4H, −SCH$_2$), 2.41 (s, 6H, C-1), 1.74 (p, 4H, C-11), 1.44 (p, 4H, C-12), 1.33 (m, 8H, C-13,14), 0.88 (t, 6H, C-15). ^{13}C NMR (125 MHz, CDCl$_3$, ppm) δ: 179.53 (C=S), 161.71(CH=N), 143.16(C-5), 131.55(C-4,6), 129.35 (C-2), 128.54(C-3,7), 35.16(C-1), 31.52(C-10), 29.54(C-11), 28.62(C-12), 22.69(C-13), 21.95(C-14), 14.20(C-15). UV–vis spectrum [CHCl$_3$, λ$_{max}$ nm (log ε, L mol^{-1} cm^{-1})]: 247(4.57), 305(4.62), 367(4.22). HRMS (FAB) Calc. for C$_{30}$H$_{43}$N$_4$S$_4$Pd (M + 1): 693.1327; Found (M + 1): 693.1404. Molar conductivity (1.0 × 10^{-5} M; CHCl$_3$, Ω^{-1} cm^2 mol^{-1}): 0.00; μ$_{eff}$ = Diamagnetic.

2.3.6. [PbL$_2$] (7)
Pale yellow, Yield: 55%; m.p. (140–142 °C). Selected IR data (KBr disk, cm^{-1}): ν(C−H, alkyl) 2924 ms, ν(C=N) 1604 s, ν(N−N) 1033 s, ν(CSS) 817. ^{1}H NMR (500 MHz, CDCl$_3$, ppm) δ: 8.08 (s, 2H, CH=N), 7.58 (d, 4H, C-4,6), 7.12 (d, 4H, C-3,7), 2.93 (t, 4H, -SCH$_2$), 2.41 (s, 6H, C-1), 1.71 (p, 4H, C-11), 1.41 (p, 4H, C-12), 1.29 (m, 8H, C-13,14), 0.87 (t,

6H, C-15). ^{13}C NMR (125 MHz, CDCl$_3$, ppm): 176.19(C=S), 162.26(CH=N), 142.51(C-5), 130.35(C-4,6), 129.96(C-2), 128.29(C-3,7), 35.38(C-1), 34.16(C-10), 31.55(C-11), 28.80(C-12), 22.75(C-13), 21.77(C-14), 14.22(C-15). UV–vis spectrum [CHCl$_3$, λ_{max} nm (log ε, L mol^{-1} cm^{-1})]: 244(4.17), 338(4.90). HRMS (FAB) Calc. for C$_{30}$H$_{43}$N$_4$S$_4$Pb (M + 1): 795.2059; Found (M + 1): 795.2125. Molar conductivity (1.0 × 10^{-5} M; CHCl$_3$, Ω^{-1} cm^2 mol^{-1}): 0.00; μ_{eff} = Diamagnetic.

2.4. X-ray data collection and structure determinations

X-ray diffraction patterns of metal complexes **3** and **4** were collected by using a Rigaku R-AXIS RAPID diffractometer equipped with CCD. The experiments were performed at 173 K with Mo Kα radiation (λ = 0.71075 Å). Cell refinement, indexing and scaling of the data sets were carried out using the Crystal Structure package (Rigaku Inc., 2010). All the structures were solved by direct methods (Sheldrick, 2008) and subsequent Fourier analyses and refined by the full-matrix least-squares method based on F^2 with all observed reflections (Sheldrick, 2008). An absorption correction was applied to the data (Rigaku Inc., 1995). The contribution of H atoms, at geometrical calculated positions, was introduced in the final cycles of refinement. Ortep drawings were done with program Cameron (Watkin et al., 1993) implemented in the WinGX package (Farrugia, 1999). Table 1 summarizes the pertinent crystallographic data and refinement details of **3** and **4**. Crystal data of ligand **1** and of complexes **2** and **6**, discussed in this work, have been reported by us elsewhere (Howlader et al., 2015a,b; Begum et al., 2015).

2.5. Computational methods

For theoretical calculations, the X-ray structure of Ni and Pd complexes (Howlader et al., 2015b; Begum et al., 2015) was considered for initial geometry. Optimization of the equilibrium structures and subsequent vibrational frequency calculations of *cis* and *trans* isomers of Ni and Pd (singlet) were performed using density functional theory employing Becke's (B3) (Becke, 1993) exchange functional combining Lee, Yang, and Parr's (LYP) correlation functional (Lee et al., 1988). To account for the relativistic effect of transition metals, all calculations were conducted by Stuttgart/Dresden (SDD) effective core potential basis set (Andrae et al., 1990; Dunning, 1989). The absence of imaginary frequencies confirmed that the stationary points correspond to minima on the potential energy surface. B3LYP hybrid functional can reproduce the experimental vibrational frequencies; however, scaling factors (0.9613–0.9688) are required for different basis sets (Merrick et al., 2007; Andersson and Uvdal, 2005; Halim et al., 2010). Since the SDD basis set has superior performance on reproducing the experimental vibrational frequencies, scaling factor of 0.9800 can provide very comparative results (Enamullah et al., 2015a). Frontier molecular orbitals of these complexes were computed at the same level of theory. Time-dependent density functional theory (TD-DFT) (Gross and Kohn, 1990; Runge and Gross, 1984; Marques and Gross, 2004) was employed with the B3LYP/SDD level of theory for calculating the photophysical properties of these complexes considering 100 excited states. All theoretical calculations were implemented by Gaussian 09 software suite (Frisch et al., 2009).

2.6. Antibacterial assay

Antibacterial activity of the above newly synthesized compounds was screened against three Gram-negative organisms: *Shigela flexneri*, *Salmonela typhi*, and *Escherichia coli* using standard procedure (Valgas et al., 2007). Solid compounds were dissolved in DMSO at a concentration of 10,000 µg mL^{-1}. Only DMSO and tetracycline were used as a negative and positive control, respectively. Each inoculum was spread uniformly in LB agar medium containing plates. Solution of each sample was poured into a round piece of sterile filter paper and after drying introduced into agar plates in triplicate. All these plates were incubated at 37 °C overnight. The plates were then examined for the zone of inhibition which indicates the degree of susceptibility or resistance of the test organisms against the applied compounds. Inhibition zones were measured with a ruler as millimeter (Gülcan et al., 2012).

3. Results and discussion

3.1. Spectroscopic characterization

As reported in Section 2.2, condensation of 4-methylbenzaldehyde with *S*-hexyldithiocarbazate gave the bidentate Schiff base ligand **1**, which like most esters of dithiocarbazones can undergo thione-thiol tautomerization,

Table 1 Crystallographic data and details of refinement for complexes **3**–**4**.

	3	4
Empirical formula	C$_{30}$H$_{42}$N$_4$S$_4$Cu	C$_{30}$H$_{42}$N$_4$S$_4$Zn
Formula mass	650.47	652.31
System	Triclinic	Monoclinic
Space group	$P\bar{1}$	$C2/c$
a (Å)	4.67630(10)	32.39325(15)
b (Å)	10.5419(4)	5.0511(5)
c (Å)	16.4622(4)	24.9170(7)
α (°)	86.6940(10)	
β (°)	85.5840(10)	127.0319(8)
γ (°)	79.2550(10)	
V (Å^3)	794.17(4)	3254.7(3)
Z	1	4
D_{calc} (Mg/m^3)	1.360	1.331
μ (mm^{-1})	0.977	1.037
$F(000)$	343	1376
θ max (°)	27.48	25.35
No. of reflections collected	7938	12,589
No. of independent reflections	3600	2967
R_{int}	0.0249	0.0265
No. of reflections $I > 2\sigma(I)$	3357	2709
Parameters refined	180	179
$R1$ ($I > 2\sigma(I)$)[a]	0.0315	0.0284
$wR2$[a]	0.0861	0.0765
Goodness of fit (F^2)	1.114	1.074
Residuals (e/Å^3)	0.528, −0.266	0.440, −0.180

[a] $R1 = \Sigma$ $||Fo| - |Fc||/\Sigma|Fo|$, $wR2 = [\Sigma w$ $(Fo^2 - Fc^2)^2/\Sigma w$ $(Fo^2)^2]$ø.
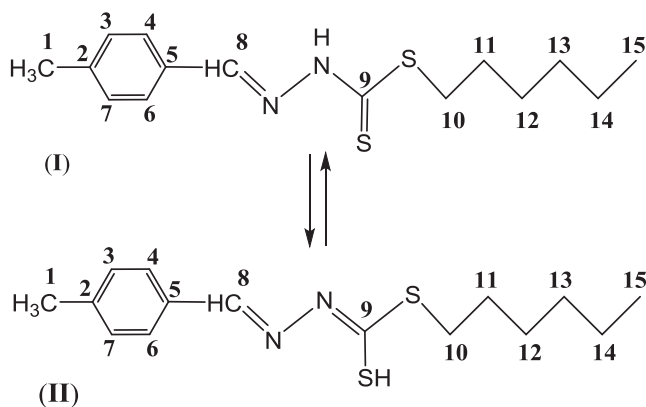
Scheme 1   Thione (I) and thiol (II) tautomeric forms of HL.

Scheme 1 (Krasowska et al., 2010). However spectroscopic data show that the Schiff base exists in solid state and in solution in its thione tautomer form. In fact IR spectrum of ligand **1** shows thioamide ν(N—H) band at 3101 cm^{-1}, but no ν (S—H) band at $\sim$2700 cm^{-1} was detected (Crouse et al., 2004; Roy et al., 2008).

The treatment of ligand with divalent metal ions in methanol is accompanied by deprotonation, leading to the formation of neutral bischelated complexes. This is reflected in the lack of the thioamide NH resonance of the ligand in the ^{1}H NMR and disappearance of the ν(N—H) bands in the IR spectra. In fact two strong bands shown by the ligand at 1619 and 1101 cm^{-1} are assigned to the ν(C=N) and ν(C=S) stretching vibrations, respectively, (Crouse et al., 2004; Chan et al., 2008) and the absence of the ν(C=S) band in the complexes is a genuine evidence for the formation of complexes *via* the enol group (Chew et al., 2004; Takjoo et al., 2010).

In the metal complexes the ν(C=N) band appeared in the range 1604–1583 cm^{-1}, thus at lower frequency with respect to the ligand, evidencing that the coordination to the metal occurred through the azomethine nitrogen (Chew et al., 2004). The calculated (scaled) frequency of the ν(C=N) band detected at 1597 cm^{-1} supports the experimental result. The shift of the stretching frequency of ν(N—N) band of the free ligand to higher wave numbers in the spectra of the complexes (from 1026 to ca. 1030 cm^{-1}) also confirms the bonding of azomethine nitrogen to the metal ions (Roy et al., 2008; Chan et al., 2008). However, the calculated ν(N—N) band is strong and shifted to 938–915 cm^{-1}. The stretching frequency of the ν(CSS) band in the complexes decreased (817–803 cm^{-1}) in comparison with that observed in the free ligand (871 cm^{-1}), indicating that complexation has taken place through the thiolate sulfur (Ali et al., 2002; Takjoo et al., 2012). A similar calculated ν(CSS) band is noticed at 802 cm^{-1}.

The ^{1}H NMR spectrum of ligand **1** showed a broad singlet at 11.01 ppm assigned to the (N—H) proton but no signal attributable to the thiol proton ($\sim$4.0 ppm) was detected, indicating the absence of this tautomer (Crouse et al., 2004; Chew et al., 2004; Khaledi et al., 2011). On the other hand, the lack of the NH signal in the ^{1}H NMR spectra of complexes **2–7** indicates that complexation occurred *via* deprotonation of this group (Islam et al., 2014) as confirmed by the X-ray crystallographic study.

The azomethine (CH=N) proton observed as a singlet at 7.93 ppm in HL, shifted at higher field (7.79–7.62 ppm) in the complexes due to the coordination of azomethine nitrogen (Takjoo et al., 2012; Khaledi et al., 2011; Islam et al., 2011, 2014; Ali et al., 2006). The signals at 3.31 and 2.42 ppm corresponding to —SCH$_2$ and C-1 in the ligand were shifted to 3.12–3.01 ppm and 2.41–2.36 ppm upon complexation (Ravoof et al., 2010; Low et al., 2014). In the ligand the signals at 1.76, 1.47, 1.34 and 0.91 ppm corresponding to C-11, C-12, C-13,14 and C-15, respectively, all show slight variation upon complexation. However, the paramagnetic electron configuration of complex **3** hampered the identification of the functional group through ^{1}H NMR spectrum (Yazdanbaksh et al., 2009). The ^{13}C NMR spectral data of the complexes in solution confirm the structure as observed in solid state by X-ray diffraction.

The room temperature molar conductance values of the complexes (10^{-5} M in CHCl$_3$ solution) are indicative of non-electrolytic nature (Crouse et al., 2004; Chew et al., 2004). The *Lassaigne's* test (halogen test) indicated the absence of chloride ions in the Pd^{II} complex **6**.

The magnetic moment of Cu^{II} complex **3** is 1.82 B.M. at room temperature corresponding to a single electron spin, (Islam et al., 2011) while all the other complexes are diamagnetic. Complexes **2** and **6** are consistent with a square planar geometry, while derivatives **4**, **5** and **7** are expected to have a tetrahedral structure (Crouse et al., 2004; Islam et al., 2011).

The High Resolution Mass Spectrum (HRMS) of ligand **1** showed a peak at m/z = 295.1302, which is consistent with the proposed formula, and the molecular ion peaks of Ni^{II}, Cu^{II}, Zn^{II}, Cd^{II}, Pd^{II} and Pb^{II} complexes (**2–7**) have m/z (M + 1) at 645.1728, 650.1664, 651.1659, 701.1411, 693.1404 and 795.2125, respectively, suggesting the formation of bischelated complexes with the ligand **1**.

The electronic spectrum of the Schiff base ligand **1** showed two bands at 241 and 262 nm, arising from $\pi \rightarrow \pi^*$ transitions for the aromatic ring and azomethine (CH=N) moiety, respectively (Islam et al., 2011). Other two bands at 325 and 338 nm are assigned to $\pi \rightarrow \pi^*$ and $n \rightarrow \pi^*$ transitions of the dithiocarbazate group (Islam et al., 2011, 2014). The complexes exhibited intra-ligand transition (Ali et al., 2006; Ravoof et al., 2010) in the range of (305–267) nm for $\pi \rightarrow \pi^*$ (CH=N).

In the UV–vis spectra of the Ni^{II}, Cu^{II}, Zn^{II} and Pd^{II} complexes the intra-ligand band ascribed to $n \rightarrow \pi^*$ transition is shifted to higher wavelength (blue shift), while it disappeared in other complexes. This is due to coordination of the thiol sulfur to the metal (Yazdanbaksh et al., 2009; Low et al., 2014). The time-dependent density functional theory (TD-DFT) calculation exhibited the intra-ligand bands at 260 and 320 nm for the *trans* isomer of NiL$_2$ while these bands are detected at 243 and 339 nm for the *cis* isomer of PdL$_2$ (Fig. 14S, supporting information). Moreover, the intra-ligand band of the *cis/trans* PdL$_2$ is very strong and broad indicating that these derivatives can show distinctive fluorescence property.

Complexes **2**, **3** and **4** showed the presence of ligand-to-metal charge transfer (LMCT) bands (443–435 nm) arising from S $\rightarrow$ M^{II} interaction (Ali et al., 2012; Crouse et al., 2004; Ravoof et al., 2010; Aazam et al., 2012; Nair and Joseyphus, 2008). The appearance of this LMCT band in these complexes is also strong evidence that the metal is coordinated by the thiol sulfur. The calculated LMCT bands for *cis* and
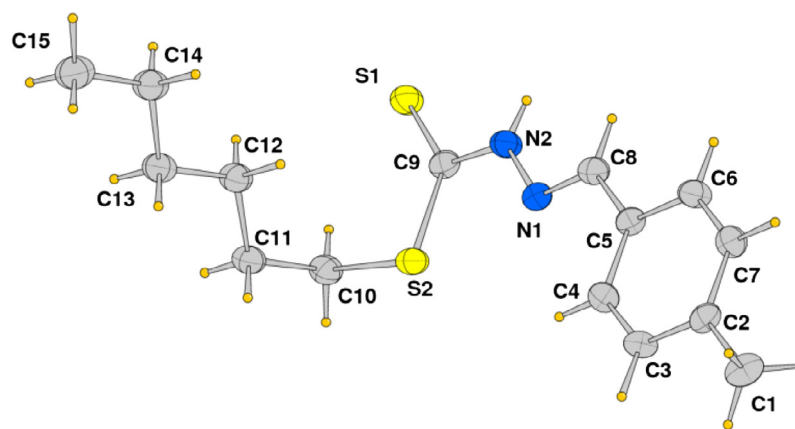
Figure 1   ORTEP drawing (50% probability ellipsoids) of ligand **1.**

Table 2   Selected bond lengths (Å) and angles (°) of HL and of the coordinated ligand in metal complexes **2**, **3**, **4** and **6**.

	Ligand	Ni (2)	*trans*-Ni (calc)	Zn (3)	Cu (4)	Pd (6)	*cis*-Pd (calc)
S1—C9	1.670(3)	1.720(4)	1.768	1.746(3)	1.7282(14)	1.777(17)	1.802
S2—C9	1.759(3)	1.757(4)	1.802	1.7493(15)	1.7529(16)	1.747(16)	1.809
S2—C10	1.814(3)	1.811(4)	1.902	1.812(3)	1.8146(16)	1.829(18)	1.903
N1—C8	1.277(3)	1.294(5)	1.514	1.290(3)	1.2931(19)	1.208(16)	1.311
N1—N2	1.375(3)	1.425(4)	1.357	1.3934(17)	1.4013(17)	1.404(17)	1.437
N2—C9	1.335(3)	1.269(5)	1.330	1.295(3)	1.288(2)	1.282(15)	1.311
N(2)—N(1)—C(8)	115.97(18)	113.8(3)	110.4	117.68(17)	116.01(12)	114.2 (12)	111.9
N(1)—N(2)—C(9)	120.61(18)	111.9(3)	115.9	113.78(17)	113.06(12)	115.8 (16)	114.1
S(1)—C(9)—S(2)	126.25(13)	113.9(3)	118.6	112.24(11)	112.82(8)	109.6 (9)	114.9
S(1)—C(9)—N(2)	120.30(17)	125.9(3)	121.0	129.76(12)	127.55(12)	125.6 (15)	125.8
S(2)—C(9)—N(2)	113.44(17)	120.2(3)	120.4	118.00(16)	119.63(11)	124.7 (15)	119.3
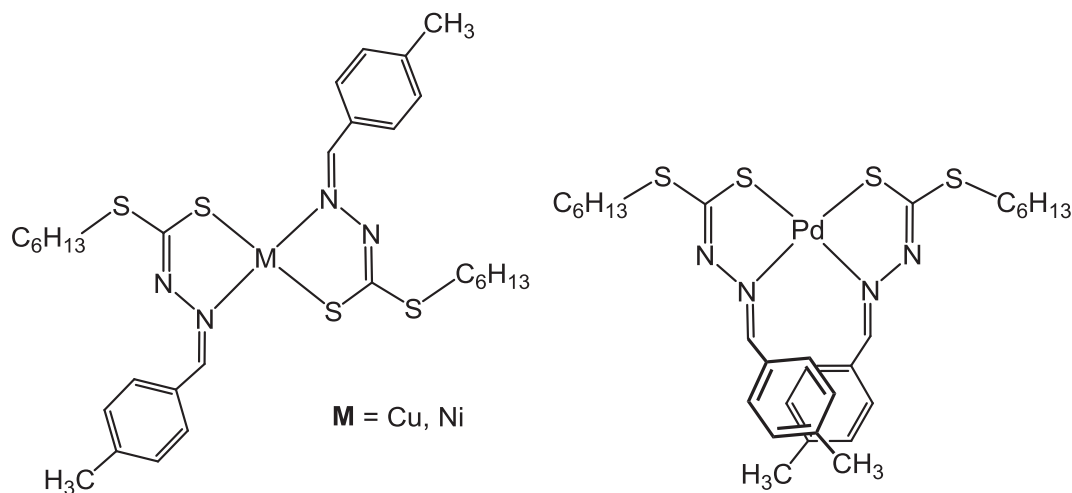
Scheme 2   The different configuration detected in square planar Cu, Ni, and Pd complexes.

trans NiL$_2$ showed a broad shoulder from 400 to 560 nm with absorption maxima at 482 nm (Fig. 14S, supporting information). This intense excitation is occurred from the highest occupied molecular orbital (HOMO−2) to lowest unoccupied molecular orbital (LUMO) (Fig. 15S, supporting information). The electronic spectra of Ni^{II} and Pd^{II} complexes having d^8 configuration are expected to exhibit three bands associated with the $^1A_{1g} \rightarrow {}^1A_{2g}$, $^1A_{1g} \rightarrow {}^1B_{1g}$, and $^1A_{1g} \rightarrow {}^1E_{1g}$ transitions. However, such transitions are difficult to distinguish as the excited states associated with d-d, LMCT and ligand-to-ligand charge transfer (LLCT) transitions are overlapped with each other and difficult to construe as the respective excited

states are fairly close in energy (Jorge et al., 2003; Enamullah et al., 2014, 2015b; Hossain et al., 2015). For cis-PdL₂, analogous LMCT shoulder is also noticed in the region of 400–500 nm with absorption maxima at 447 nm.

3.2. Structural descriptions

An Ortep drawing of the ligand, depicted in Fig. 1, shows the molecule in its thione tautomeric form. With exception of the S-hexyl chain, all the atoms are co-planar, indicating an electron delocalization within the molecule. Dithiocarbazate compounds can exist as E or Z diastereoisomers as already noted years ago (Lanfredi et al., 1977) and in the present case the molecule adopts an E configuration with respect to the C(8)=N(1) bond of the benzylidene fragment, while the β-nitrogen and the thioketo sulfur are *trans* located with respect to the N(2)−C(9) bond. The bond lengths and angles of **1** compare well with those measured in several related structures (Tarafder et al., 2008, 2010). It is worth noting that upon coordination the molecule requires a 180° rotation about the C9−N2 bond in order to chelate the metal through the N1, S1 donors.

The structural determination of the series of metal complexes allows to compare the bond distances and angles of the HL with the correspondent geometrical parameters measured in the metal complexes. Inspection of Table 2 indicates some salient differences in the coordinated ligand compared to the free ligand, and the most obvious are as follows: (i) a significant elongation of the S(1)−C(9) bond length (range 1.720(4)–1.777(17) Å), to be compared to the value of 1.670(3) Å in HL, which validates the deprotonation of the thiolate group; (ii) a shortening of the N(2)−C(9) bond length to 1.269(5)–1.295(3) Å, (1.335(3) Å in HL), and (iii) a slight lengthening of the N(1)−N(2) bond length to 1.3934(17)–1.425(5) Å,

(1.375(3) Å in HL). Correspondingly the bond angles exhibit variations as well, particularly in the N(1)−N(2)−C(9) and S(1)−C(9)−S(2) values as reported in Table 2.

In all the metal complexes the two ligands, in their deprotonated imino thiolate form, act as chelating ligands via the azomethine nitrogen N1 and thiolate sulfur S1 atoms. However a different arrangement has been observed in square planar complexes, namely a *cis* or *trans* configuration (Scheme 2).

Nickel(II) and copper(II) complexes **2** and **3** are isomorphous and the X-ray structural analysis shows the metal located on a crystallographic center of symmetry in a square-planar coordination geometry and the observed *trans* configuration of donor atoms is imposed by the crystal symmetry. Fig. 2 shows an ORTEP view of complex **3**, while a selection of bond lengths and angles is reported in Table 3. The coordination bond distances are found slightly longer for the copper than the nickel derivative for the larger ionic radius of this metal (Shannon, 1976): Cu−N(1) = 2.0292(12), Cu−S(1) = 2.2575(4) Å, *vs.* Ni−N(1) = 1.933(3), Ni−S(1) = 2.1775(10) Å.

On the other hand in complex **6** the Pd atom resides on a crystallographic twofold axis and the two Schiff base ligands coordinate the metal center in an unexpected, although not novel, *cis*-planar configuration (Scheme 2 and Fig. 3). This coordination arrangement is accompanied by an E configuration about the N(1)=C(8) imine bond with a N2−N1−C8−C5 torsion angle of 172.1(14)°, to be compared with the mean value measured in the other metal derivatives of ca. 0.7°. This feature leads to a weak π-π interaction between the rings of the methylbenzylidene moieties, with a centroid-to-centroid distance of 4.114(8) Å. In addition the complex assumes a step conformation, which is characterized by the dihedral angles between the SCNN and the N₂S₂ mean planes of 23.47°, while the two SCNN planes form an angle of 11.56°
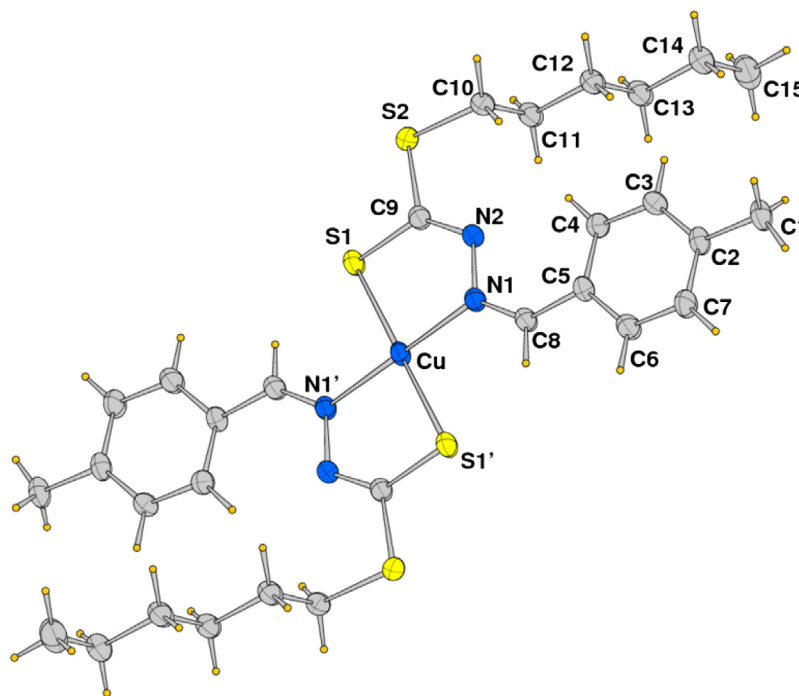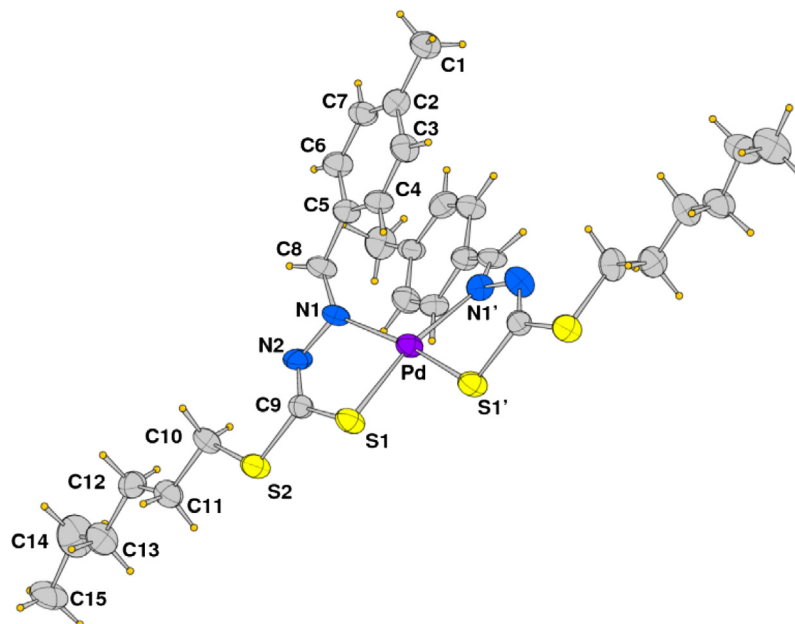

Figure 2 ORTEP drawing (50% probability ellipsoids) of Cu^II complex **3** (only labels of the independent crystal moiety are indicated). The same label scheme applies also to Ni^II complex **2**.

Table 3 Coordination bond lengths (Å) and angles (°) for metal complexes **2**, **3**, **4** and **6**.

	2 M=Ni	**2 (calc)** M=Ni	**3** M=Cu	**4** M=Zn	**6** M=Pd	**6 (calc)** M=Pd
M—N1	1.933(3)	1.848	2.0292(12)	2.0297(18)	2.154(12)	2.098
M—S1	2.1775(10)	2.248	2.2575(4)	2.2818(4)	2.264(4)	2.364
N1—M—S1	86.04(9)	87.04	84.64(4)	87.01(4)	83.2(3)	82.74
N1—M—S1′	93.96(9)	94.46	95.36(4)	119.02(5)	168.1(3)	169.46
N1—M—N1′	180.0	171.24	180.0	119.60(7)	107.1(6)	103.66
S1—M—S1′	180.0	158.80	180.0	129.02(3)	87.3(2)	92.23

Symmetry code for primed atoms: −x, −y, −z for **2** and **3**; −x, y, 1/2 − z for **4**; 1 − x, y, −z for **6**.

Figure 3 ORTEP drawing (50% probability ellipsoids) of Pd^{II} complex **6** (only labels of the independent crystal moiety are indicated).
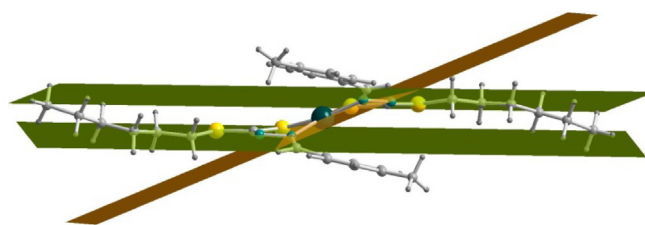
Figure 4 A perspective view of Pd^{II} complex showing the step conformation of the coordination plane with respect to the SCNN planes.

(Fig. 4). The Pd—S1 bond length is of 2.264(4) and the Pd—N1 of 2.154(12) Å, which is the longest among the complexes reported. A similar arrangement in solid state has been found also in the bischelated PdL′$_2$ complex (L′ = S-Methyl-3-(fluoren-9-ylidene)dithiocarbazate) (Zhou et al., 2007) where a π–π stacking interaction is realized between the two diazafluorene moieties.

Although different configurations of square planar metal complexes have been reported as mentioned above, we decided to evaluate the equilibrium geometry of the cis and trans complexes for Ni and Pd calculated at B3LYP/SDD level of theory. In case of cis and trans Ni(II) complexes (Fig. 5), computations revealed that the trans isomer adopts a square planar geometry, whereas the cis species showed a distorted shape. The relative enthalpy and Gibbs free energy of the cis and trans isomers are −29.12 and −43.97 kJ/mol, respectively, which indicate that the latter is more stable.

The calculated Pd—S(1) and Pd—N1 bond lengths for the cis isomer are 2.364 and 2.098 Å, respectively, vs. values of 2.419 Å and 2.057 Å for the trans species (Fig. 6). The relative enthalpy (−4.37 kJ/mol) and Gibbs free energies (−5.50 kJ/mol) of the cis isomer revealed that this is slightly more stable than the trans one.

The structural characterization of the Zn^{II} complex **4** (ORTEP view shown in Fig. 7) indicates the metal located on a crystallographic twofold rotation axis with formation of a tetrahedral coordination geometry. The dihedral angle formed by the two SCNN ring planes is of 85.03°. Here the Zn—N1 coordination bond distance (2.0297(18) Å) is comparable to that of the copper derivative, while the Zn—S(1) is slightly longer, of 2.2818(4) Å.
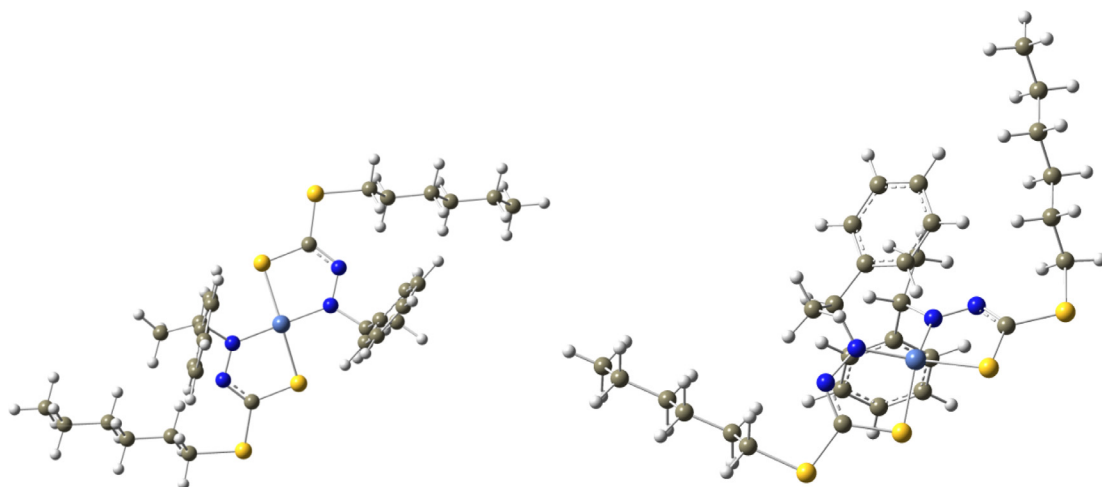
Figure 5   The equilibrium structures of *trans* and *cis* isomers of Ni complex calculated at B3LYP/SDD level of theory.
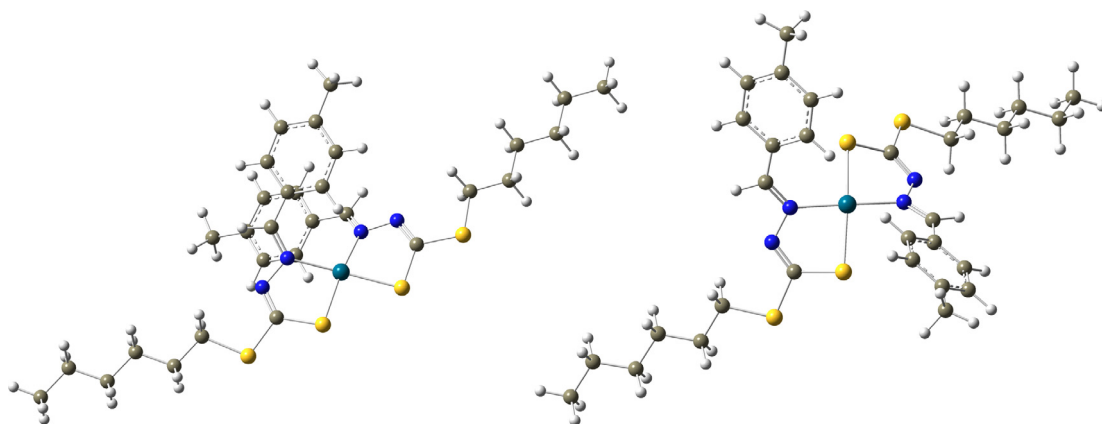

Figure 6   The equilibrium structures of *cis* and *trans* isomers of Pd complex calculated at B3LYP/SDD level of theory.

In conclusion the structural results on metal complexes indicate a similar chelation of ligands in complexes **2**, **3** and **4**, but for palladium species **6** a different configuration is observed about the N(1)=C(8) bond. However more significant is the configuration of ligands in the square planar geometry, being *cis* in Pd^{II} complex and *trans* in the Ni^{II} and Cu^{II} derivatives. Inspection of crystal packing does not provide additional information: the Ni^{II} and Cu^{II} complexes stack in the crystal at a distance of 4.675 Å (mean value of axis *a*), which exclude significant π interactions among the phenyl rings, while in the Pd^{II} crystal, the mentioned stacking interaction about aromatic rings does not seem to account for the observed *cis* arrangement, since the acetone Schiff base of *S*-methyl Pd derivative assumes a *cis*-square planar structure as well (Ali et al., 2002). A structural analysis of *trans*- and *cis*-planar nickel and copper complexes has been recently reported (Zangrando et al., 2015).

3.3. Fluorescence spectral study

The photoluminescence properties of ligand **1** and of its metal complexes **2–7** were studied using 10^{-5} M solution of CHCl$_3$ at room temperature. Upon excitation at $\lambda = 338$ nm, the emission spectrum of the ligand shows three emission peaks at $\lambda_{max} = 406$, 430 and 452 nm (Table 4 and Fig. 8). Excitation of the metal complexes at 305–376 nm gives three emission peaks in the range 396–460 nm. The emission spectral profile of all the complexes closely resembles that of the ligand.

It is evident from Fig. 8 that the fluorescence intensity of the ligand significantly decreased upon complexation for complexes **2–6** with the exception of the derivative **7**. Metal ions can enhance or quench the fluorescence intensity of some Schiff base ligands containing an aromatic ring. The formation of coordination complexes induces an energy transfer from the excited state of the ligand to the metal ions causing a decrease of the fluorescence intensity (Ravoof et al., 2010). Quenching of fluorescence intensity of a ligand by transition metal ions upon complexation is a rather common phenomenon which is explained by processes such as magnetic perturbation, redox activity, and electronic energy transfer (Singh et al., 2009; Takjoo et al., 2012; Önal et al., 2011; Anitha et al., 2013). Enhancement of fluorescence intensity through complexation is, however, of much interest as it opens up the opportunity for photochemical applications of these complexes. The fluorescence intensity of the uncoordinated ligand is probably quenched by the occurrence of a photo induced electron transfer (PET) process due to the presence of the lone pair of the donor atoms. Such PET process is prevented by the complex-
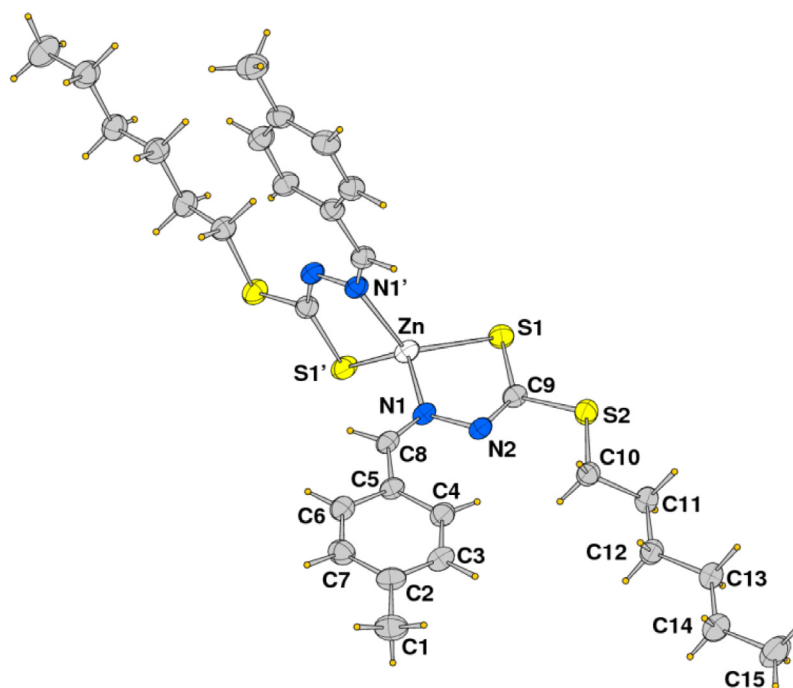
Figure 7 ORTEP drawing (50% probability ellipsoids) of Zn^{II} complex **4** (only labels of the independent crystal moiety are indicated).

Table 4 Excitation wavelength dependent emissions of compounds **1–7**.

Compound	Excitation wavelength (nm)	Emission wavelength (nm)
1	338	406, 430, 452
2	338	406, 430, 453
3	376	407, 430, 460
4	355	396, 441
5	376	406, 430, 453
6	305	340, 405, 429
7	338	406, 430, 459

Figure 8 Emission spectra of compounds **1–7** (10^{-5} M solution in $CHCl_3$) at room temperature.

ation of ligand with the metal ions; thus, the fluorescence intensity may be greatly enhanced upon coordination. The chelation of the ligand to the metal increases the rigidity of the ligand and thus reduces the loss of energy by thermal vibration decay (Konar et al., 2011).

3.4. Electrochemical studies

The potential scanning of Ni^{II}, Cu^{II}, Pd^{II} and Pb^{II} complexes was performed using a Pt disk electrode (2 mm in diameter) in the presence of tetra-*n*-butylammonium tetrafluoroborate as supporting electrolyte at a scan rate of 50 mV s^{-1}. A Pt wire and Ag/AgCl (sat. KCl) were used to serve as reference and counter electrode, respectively. We excluded Zn^{II} and Cd^{II} complexes from the electrochemical study for their stable oxidation state (Zn^{2+} and Cd^{2+} possess 3d^{10} and 4d^{10} configuration, respectively), that makes these metal centers reluctant to a redox behavior.

Cyclic voltammograms (CVs) of N_2 purged solutions of Ni^{II}, Cu^{II}, Pd^{II}, and Pb^{II} complexes are shown in Fig. 9, indicating that from 0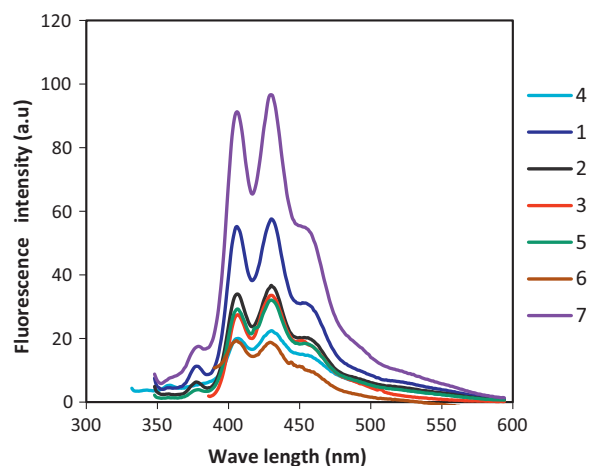 to -0.6 V no peak was generated in the absence of the metal complex. No peak was also observed for Pd^{II} and Pb^{II} complexes. Scanning the 1.0×10^{-3} M Ni^{II} complex solution, an irreversible weak peak was fashioned at -0.34 V. However, the addition of Cu^{II} complex to the supporting electrolyte, produced two peaks during forward and reverse scan, respectively. The potential difference ($E_{pa} - E_{pc}$) of ca. 230 mV and peak current ratio (I_{pc}/I_{pa}) of 3.5 indicate that the redox process for complex **3** is a quasi-reversible one electron transfer process under the experimental conditions. During cathodic scan at -0.39 V, Cu^{II} is reduced to Cu^{I} providing highly intense wave. However, when the potential scanning was reverted from -0.6 V, an anodic wave developed giving maximum intensity at -0.16 V corresponding to the re-oxidation of Cu^{I} to Cu^{II} species. It was observed that even
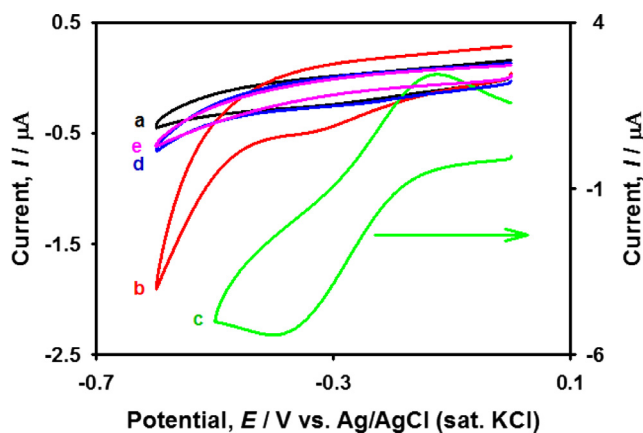
Figure 9 Cyclic voltammograms of 1.0×10^{-1} M $(n\text{-}Bu)_4N]BF_4$ at a Pt disk electrode in the absence (a) and presence of 1.0×10^{-3} M Ni^{II} (b), Cu^{II} (c), Pd^{II} (d), and Pb^{II} (e) complex in $CHCl_3$. Scan rate: 50 mV s^{-1}.
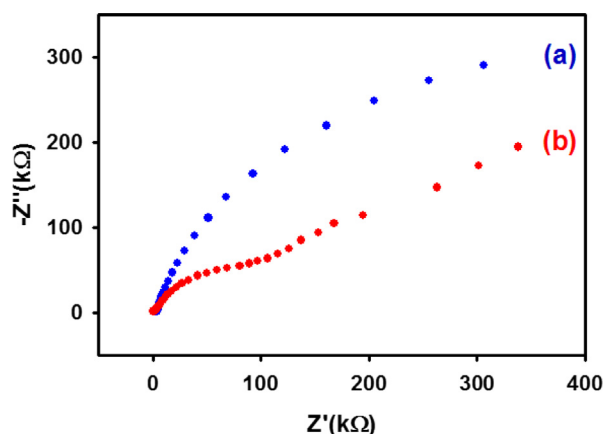

Figure 10 Nyquist plot of Pt electrode in 1.0×10^{-1} M $[(n\text{-}Bu)_4N]BF_4$ solution in absence (a) and presence (b) of 1.0×10^{-3} M Cu^{II} complex at -0.45 V.

at faster scan rates ($v > 100$ mV s^{-1}), the I_{pc}/I_{pa} ratio was not significantly altered. This observation suggests that the reduced Cu^{I} complex was probably unstable at the cathodic

Table 5 Inhibition zone diameter (mm) induced by newly synthesized compounds against *Escherichia coli*, *Salmonella typhi* and *Shigella flexneri* bacteria (conc. = 400 μg disk^{-1}).

Ligand/complex	*Escherichia coli*	*Salmonella typhi*	*Shigella flexneri*
1	6	7	7
2	–	–	–
3	10	–	–
4	–	–	–
5	8	–	–
6	7	–	–
7	12	–	–
Negative control	–	–	–
Tetracycline	32	31	38

potential and underwent some irreversible chemical or structural changes. Less cathodic peak current for Ni^{II} complex indicates the relative stability of this complex over Cu containing species, whereas Pd^{II} and Pb^{II} complexes do not undergo any outer sphere redox reaction indicating that neither ligands nor metal centers are adsorbed on the electrode surface under the experimental conditions.

In order to ensure the electron transfer properties, electrochemical impedance spectra (EIS) measurements were then carried out at -0.45 V within the frequency range from 0.01 to 100 kHz. The Nyquist plots and the corresponding Bode module and phase are displayed in Figs. 10 and 11, respectively. The higher frequency impedance indicates solution resistance (R_s) and the impedance, due to higher AC frequency, corresponds to the resistance due to the electron transfer (R_{et}). A rise of the impedance after the arc of the semicircle (at lower AC frequency region) indicates a diffusion process. According to Fig. 10, the $[(n\text{-}Bu)_4N]BF_4$ supporting electrolyte imparted higher electron transfer resistance both in the imaginary and in the real parts of the EIS spectra. When the spectrum was recorded in the presence of Cu^{II} complex 3, an arc evolved. By considering the diameter of the arc (associated to the real part of the semicircle) it was confirmed that an easy electron transfer occurred from the electrode surface to the redox center of the metal complex, with a R_{et} value of ca. 100 kΩ.
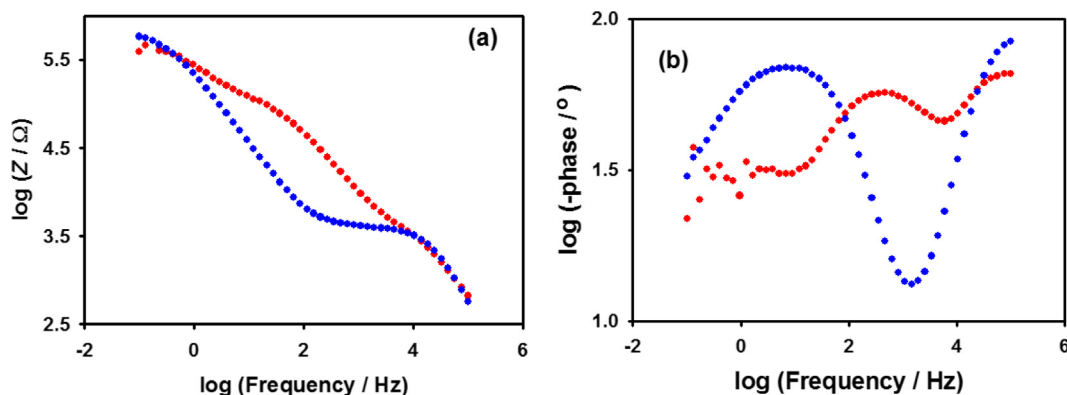

Figure 11 Bode module (a) and bode phase (b) diagrams of the Nyquist plot of $[(n\text{-}Bu)_4N]BF_4$ at Pt disk electrode in absence (blue dotted lines) and presence (red dotted limes) of Cu^{II} complex at -0.45 V.

3.5. Biological activity

Biological activity of the present compounds in terms of anti-bacterial property was analyzed against three well known pathogenic Gram-negative organisms such as *Escherichia coli*, *Salmonella typhi* and *Shigella flexneri*. All these three micro-organisms are member of enterobacteriaceae family and caused several diseases of human including diarrhea, typhoid, and food poisoning. Thus, it is worth to evaluate the anti-bacterial property of our newly synthesized compounds against these three common pathogenic micro-organisms. The activity was tested after dissolution of all the compounds **1–7** in DMSO, which was used as a negative control in the experiment. Tetracycline, a broad-spectrum second generation antibiotic, was used as positive anti-bacterial compound. The results of the bacterial growth inhibition are shown in Table 5 along with the corresponding positive and negative controls. There was no growth of inhibition for negative control, whereas positive control (tetracycline) showed significant growth inhibition (31–38 mm) against all these three tested organisms, indicating that the experimental set and procedures are appropriate for the test. Among the synthesized compounds, only the free ligand **1** showed anti-bacterial activity against all three tested organisms with an inhibition zone of 6–7 mm. With this exception, compounds **3**, **5**, **6** and **7** showed distinguishable inhibition zone against *E. coli* only, with complex **7** exhibiting the largest inhibition zone (12 mm). According to these results, all the compounds, except **2** and **4**, possess some level of antibacterial activity that could be explored further, obviously taking into account that Pb and Cd cause adverse health effects in humans and animals (Naja and Volesky, 2009).

4. Conclusion

A detailed investigation, that comprises density functional calculations, photoluminescence, electrochemical studies and antimicrobial activity, has been performed on a series of bischelated complexes with dithiocarbazate Schiff base ligand bearing a long alkyl chain. The ligand acts as chelating species coordinating the metal through the azomethine nitrogen and the thiolate sulfur atoms in all the complexes. The X-ray diffraction study of the Ni[II], Cu[II], Zn[II] and Pd[II] complexes indicates square planar or tetrahedral coordination geometry and in the former case either a *cisoid* or *transoid* configuration. DFT calculations confirmed that *trans* configuration of NiL$_2$ and *cis* configuration of PdL$_2$ appears more stable compared to the other configurational isomer, although packing forces are not to be excluded in driving the preferential configuration isolated in solid state. The stability of complexes and a certain degree of antibacterial activity justify further studies to establish correlations between bioactivity of this class of compounds with both their solid and solution structures as well as their redox properties.

Acknowledgments

Appendix A. Supplementary material

^{1}H and ^{13}C NMR spectra, Uv–vis spectra, HRMS of compounds **1–7**. ORTEP drawing of complex **2**. TD-DFT spectra of complexes **2** and **6** and HOMO, LUMO diagrams for *trans* NiL$_2$ complex. CCDC 1057811 and 1403800 contain the supplementary crystallographic data for this paper. These data can be obtained free of charge from The Cambridge Crystallographic Data Centre via www.ccdc.cam.ac.uk/data_request/cif.

Supplementary data associated with this article can be found, in the online version, at http://dx.doi.org/10.1016/j.arabjc.2016.07.019.

References

Aazam, E.S., EL Husseiny, A.F., Amri, H.M.A., 2012. Arab. J. Chem. 5, 45–53.

Ali, M.A., Mirza, A.H., Butcher, R.J., Tarafder, M.T.H., Keat, T.B., Ali, A.M., 2002. J. Inorg. Biochem. 92, 141–148.

Ali, M.A., Mirza, A.H., Butcher, R.J., Crouse, K.A., 2006. Transition Met. Chem. 31, 79–87.

Ali, M.A., Tan, A.L., Mirza, A.H., Santos, J.H., Abdullah, A.H.B.H., 2012. Transition Met. Chem. 37, 651–659.

Andersson, M.P., Uvdal, P., 2005. J. Phys. Chem. Sect. A 109, 2937–2941.

Andrae, D., Häussermann, U., Dolg, M., Stoll, H., Preuss, H., 1990. Theor. Chim. Acta 77, 123–141.

Anitha, C., Sheela, C.D., Tharmaraj, P., Shanmugakala, R., 2013. Int. J. Inorg. Chem., 1–10 436275

Becke, A.D., 1993. J. Chem. Phys. 98, 1372–1377.

Begum, M.S., Howlader, M.B.H., Sheikh, M.C., Miyatake, R., Zangrando, E., 2015. Acta Cryst. Sect E 71, m63–m64.

Beshir, A.B., Guchhait, S.K., Gascon, J.A., Fenteany, G., 2008. Bioorg. Med. Chem. Lett. 18, 498–504.

Chan, M.H.E., Crouse, K.A., Tahir, M.I.M., Rosli, R., Umar-Tsafe, N., Cowley, A.R., 2008. Polyhedron 27, 1141–1149.

Chew, K.-B., Tarafder, M.T.H., Crouse, K.A., Ali, A.M., Yamin, B.M., Fun, H.-K., 2004. Polyhedron 23, 1385–1392.

Crouse, K.A., Chew, K.-B., Tarafder, M.T.H., Kasbollah, A., Ali, A.M., Yamin, B.M., Fun, H.-K., 2004. Polyhedron 23, 161–168.

da S. Maia, P.I., de A. Fernandes, A.G., Silva, J.J.N., Andricopulo, A.D., Lemos, S.S., Lang, E.S., Abram, U., Deflon, V.M., 2010. J. Inorg. Biochem. 104, 1276–1282.

Dunning, T.H., 1989. J. Chem. Phys. 90, 1007–1023.

Enamullah, M., Uddin, A.K.M.R., Pescitelli, G., Berardozzi, R., Makhloufi, G., Vasylyeva, V., Chamayou, A.-C., Janiak, C., 2014. Dalton Trans. 43, 3313–3329.

Enamullah, M., Islam, M.K., Halim, M.A., Janiak, C., 2015a. J. Mol. Struct. 1099, 154–162.

Enamullah, M., Quddus, M.A., Halim, M.A., Islam, M.K., Vasylyeva, V., Janiak, C., 2015b. Inorg. Chim. Acta 427, 103–111.

Farrugia, L.J., 1999. J. Appl. Crystallogr. 32, 837–838.

Frisch M.J. et al., 2009. Gaussian 09, Revis. A. 02.

Groom, C.R., Bruno, I.J., Lightfoot, M.P., Ward, S.C., 2016. Acta Cryst. Sect B 72, 171–179.

Gross, E.K.U., Kohn, W., 1990. Adv. Quantum Chem. 21, 255–291.

Gülcan, M., Sönmez, M., Berber, İ., 2012. Turk. J. Chem. 36, 189–200.

Halim, M.A., Shaw, D.M., Poirier, R.A., 2010. J. Mol. Struct. Theochem. 960, 63–72.

Hossain, M.E., Hasan, M.M., Halim, M.E., Ehsan, M.Q., Halim, M. A., 2015. Spectrochim. Acta Part A Mol. Biomol. Spectrosc. 138, 499–508.

Howlader, M.B.H., Begum, M.S., Sheikh, M.C., Miyatake, R., Zangrando, E., 2015a. Acta Cryst. Sect E 71, o103–o104.

Howlader, M.B.H., Begum, M.S., Sheikh, M.C., Miyatake, R., Zangrando, E., 2015b. Acta Cryst. Sect E 71, m26–m27.

Islam, M.A.A.A.A., Tarafder, M.T.H., Sheikh, M.C., Alam, M.A., Zangrando, E., 2011. Transition Met. Chem. 36, 531–537.

Islam, M.A.A.A.A., Sheikh, M.C., Alam, M.S., Zangrando, E., Alam, M.A., Tarafder, M.T.H., Miyatake, R., 2014. Transition Met. Chem. 39, 141–149.

Jorge, F.E., Autschbach, J., Ziegler, T., 2003. Inorg. Chem. 42, 8902–8910.

Khaledi, H., Ali, H.M., Olmstead, M.M., 2011. Inorg. Chim. Acta 366, 233–240.

Konar, S., Jana, A., Das, K., 2011. Polyhedron 30, 2801–2808.

Krasowska, M., Kochel, A., Filarowski, A., 2010. CrystEngComm 12, 1955–1962.

Lee, C., Yang, W., Parr, R.G., 1988. Phys. Rev. Sect B 37, 785–789.

Lanfredi, A.M.M., Tiripicchio, A., Camellini, M.T., Monaci, A., Tarli, F., 1977. J. Chem. Soc., Dalton Trans., 417–422

Low, M.L., Maigre, L., Dorlet, P., Guillot, R., Pagès, J.-M., Crouse, K.A., Policar, C., Delsuc, N., 2014. Bioconjugate Chem. 25, 2269–2284.

Marques, M.A.L., Gross, E.K.U., 2004. Annu. Rev. Phys. Chem. 55, 427–455.

Merrick, J.P., Moran, D., Radom, L., 2007. J. Phys. Chem. Sect A 111, 11683–11700.

Nair, M.S., Joseyphus, R.S., 2008. Spectrochim. Acta Sect A 70, 749–753.

Naja, G.M., Volesky, B., 2009. Toxicity and sources of Pb, Cd, Hg, Cr, As, and radionuclides in the environment. In: Shammas, N.K., Hung, Y.-T., Chen, J.P., Wang, L.K. (Eds.), Heavy Metals in the Environment. CRC Press, pp. 13–61.

Önal, Z., Zengin, H., Sönmez, M., 2011. Turk. J. Chem. 35, 905–914.

Pavan, F.R., da S. Maia, P.I., Leite, S.R.A., Deflon, V.M., Batista, A. A., Sato, D.N., Franzblau, S.G., Leite, C.Q.F., 2010. Eur. J. Med. Chem. 45, 1898–1905.

Rigaku Inc., 1995. ABSCOR. Rigaku Corporation, Tokyo, Japan.

Rigaku Inc., 2010. Crystal Structure. Version 4.0. Rigaku Corporation, Tokyo, Japan.

Ravoof, T.B.S.A., Crouse, K.A., Tahir, M.I.M., How, F.N.-F., Rosli, R., Watkins, D.J., 2010. Transition Met. Chem. 35, 871–876.

Richardson, D.R., Sharpe, P.C., Lovejoy, D.B., Senaratne, D., Kalinowski, D.S., Islam, M., Bernhardt, P.V., 2006. J. Med. Chem. 49, 6510–6521.

Roy, S., Mandal, T.N., Barik, A.K., Pal, S., Gupta, S., Butcher, R.J., Nethaji, M., Kar, S., 2008. Polyhedron 27, 593–601.

Runge, E., Gross, E.K.U., 1984. Phys. Rev. Lett. 52, 997.

Shannon, R.D., 1976. Acta Cryst. Sect A 32, 751–767.

Sheldrick, G.M., 2008. Acta Cryst. Sect A 64, 112–122.

Singh, N.K., Kushawaha, S.K., Bharty, M.K., Dulary, R., Butcher, R. J., 2009. J. Mol. Struct. 936, 257–263.

Takjoo, R., Takjoo, R., Yazdanbakhsh, M., Kaju, A.A., Yaguang, C., 2010. Chin. J. Chem. 28, 221–228.

Takjoo, R., Centore, R., Rhyman, L., Ramasami, P., 2012. J. Coord. Chem. 65, 1569–1579.

Tampouris, K., Coco, S., Yannopoulos, A., Koinis, S., 2007. Polyhedron 26, 4269–4275.

Tarafder, M.T.H., Crouse, K.A., Islam, M.T., Chantrapromma, S., Fun, H.-K., 2008. Acta Cryst. Sect E 64, o1042–o1043.

Tarafder, M.T.H., Khan, S.S., Islam, M.A.A.A.A., Lorenzi, L., Zangrando, E., 2010. Acta Cryst. Sect E 66, o2851.

Watkin, D.M., Pearce, L., Prout, C.K., 1993. CAMERON. Chemical Crystallography Laboratory, University of Oxford.

Valgas, C., de Souza, M.S., Smânia, E.F.A., Smânia Jr., A., 2007. Braz. J. Microbiol. 38, 369–380.

Yu, Y., Kalinowski, D.S., Kovacevic, Z., Siafakas, A.R., Jansson, P.J., Stefani, C., Lovejoy, D.B., Sharpe, P.C., Bernhardt, P.V., Richardson, D.R., 2009. J. Med. Chem. 52, 5271–5294.

Wise, C.F., Liu, D., Mayer, K.J., Crossland, P.M., Hartley, C.L., McNamara, W.R., 2015. Dalton Trans. 44, 14265–14271.

Yazdanbaksh, M., Takjoo, R., Frank, W., Agahi kaju, A., 2009. J. Coord. Chem., 1–10

Zangrando, E., Islam, M.T., Islam, M.A.A.A.A., Sheikh, M.C., Tarafder, M.T.H., Miyatake, R., Zahan, R., Hossain, M.A., 2015. Inorg. Chim. Acta 427, 278–284.

Zhou, H.-P., Li, D.-M., Wang, P., Cheng, L.-H., Gao, Y.-H., Zhu, Y.-M., Wu, J.-Y., Tian, Y.-P., Tao, X.-T., Jiang, M.-H., Fun, H.-K., 2007. J. Mol. Struct. 826, 205–210.